Peri-Adventitial Delivery of Smooth Muscle Cells in Porous Collagen Scaffolds for Treatment of Experimental Abdominal Aortic Aneurysm

Journal:	*Biomaterials Science*
Manuscript ID	BM-ART-05-2021-000685.R2
Article Type:	Paper
Date Submitted by the Author:	01-Sep-2021
Complete List of Authors:	Mulorz, Joscha; Stanford University Shayan, Mahdis; Stanford University, Cardiothoracic Surgery Hu, Caroline; VA Palo Alto Health Care System, Alcazar, Cynthia; VA Palo Alto Health Care System Chan, Alex; Stanford University, Cardiothoracic Surgery Briggs, Mason; Stanford University Wen, Yan; Stanford University Walvekar, Ankita; San Jose State University Ramasubramanian, Anand; San Jose State University, Chemical Engineering Spin, Joshua; VA Palo Alto Health Care System Chen, Bertha; Stanford University Tsao, Philip; Stanford University Huang, Ngan; Stanford University, Cardiothoracic Surgery

SCHOLARONE™
Manuscripts

Peri-Adventitial Delivery of Smooth Muscle Cells in Porous Collagen Scaffolds for Treatment of Experimental Abdominal Aortic Aneurysm

Joscha Mulorz [1,2,4,5#], **Mahdis Shayan**[1,3,5#], **Caroline Hu**[1], **Cynthia Alcazar**[1], **Alex H.P. Chan**[1,3,5], **Mason Briggs**[6], **Yan Wen**[6], **Ankita P. Walvekar**[7], **Anand K. Ramasubramanian**[7], **Joshua M. Spin** [1,2,5], **Bertha Chen**[6], **Philip S. Tsao**[1,2,5], **Ngan F. Huang***[1,3,5]

[1.] Veterans Affairs Palo Alto Health Care System, Palo Alto, CA, USA
[2.] Division of Cardiovascular Medicine, Stanford University School of Medicine, Stanford, CA, USA
[3.] Department Cardiothoracic Surgery, Stanford University School of Medicine, Stanford, CA, USA
[4.] Department of Vascular and Endovascular Surgery, Medical Faculty and University Hospital Düsseldorf, Heinrich-Heine-University, Düsseldorf, Germany
[5.] Stanford Cardiovascular Institute, Stanford University, Stanford, CA, USA
[6.] Stanford University School of Medicine, Department of Obstetrics and Gynecology, Stanford, CA, USA
[7.] Department of Chemical Engineering, San Jose State University, San Jose, CA, USA

[#] Contributed equally
*Correspondence: ngantina@stanford.edu

Abstract: Abdominal aortic aneurysm (AAA) is associated with the loss of vascular smooth muscle cells (SMCs) within the vessel wall. Direct delivery of therapeutic cells is challenging due to impaired mechanical integrity of the vessel wall. We hypothesized that human-derived therapeutic cells seeded within porous collagen scaffolds can be localized to the lesion. The purpose was to we evaluate if this cell delivery approach can abrogate progressive expansion in a mouse model of AAA. Collagen scaffolds seeded with either primary human aortic SMC or induced pluripotent stem cell derived-smooth muscle progenitor cells (iPSC-SMP) had >80% *in vitro* cell viability and >75% cell penetrance through the scaffold's depth, while preserving smooth muscle phenotype. The cell-seeded scaffolds were successfully transplanted onto the murine aneurysm peri-adventitia on day 7 following AAA induction using pancreatic porcine elastase infusion. Ultrasound imaging revealed that SMC-seeded scaffolds significantly reduced the aortic diameter by 28 days, compared to scaffolds seeded with iPSC-SMPs or without cells (acellular scaffold), respectively. Bioluminescence imaging demonstrated that both cell-seeded scaffold groups had cellular localization to the aneurysm but a decline in survival with time. Histological analysis revealed that both cell-seeded scaffold groups had more SMC retention and less macrophage invasion into the medial layer of AAA lesions, when compared to the acellular scaffold treatment group. Our data suggest that scaffold-based SMC delivery is feasible and may constitute a platform for cell-based AAA therapy.

Keywords: Aortic aneurysm, smooth muscle cells, induced pluripotent stem cells, scaffold, translational model

1. Introduction

Abdominal Aortic Aneurysm (AAA) is a vascular disease that affects up to 12% of individuals over the age of 75 years in the US[1]. It is characterized by the progressive dilation of the abdominal aorta, eventually leading to rupture with a high mortality rate[2,3]. Currently no targeted drug therapies exist to limit progression, leaving patients with only open or endovascular surgical repair once the aneurysm exceeds surgical cutoff diameters[3]. A key feature of AAA is the degradation of extracellular matrix (ECM) components and disappearance of the organized layers of vascular smooth muscle cells (SMC)[4,5]. Since aortic SMCs are responsible for maintaining ECM components such as elastin and collagen fibers, their loss is closely associated with mechanical failure of the blood vessel[6].

To regenerate cellular and acellular components in AAAs, cell-based translational approaches have been tested, mostly focusing on mesenchymal stem cell (MSC) delivery[7,8]. However, given the limited ability of MSCs to differentiate into a functional smooth muscle lineage, transplanted human SMCs represent an option to replace the loss of native SMCs in AAA tissue. In contrast to MSCs, human SMCs are contractile, and SMCs can also be derived from human induced pluripotent stem cells (iPSCs)[9]. Many studies on iPSC-derived smooth muscle progenitor cells (iPSC-SMP) in tissue regeneration are underway, and published data supports their potential to repair dysfunctional smooth muscle in multiple tissue systems[10,11].

Besides the choice of therapeutic cell type, the vehicle for cellular delivery is also an important area of consideration. Since the site of aneurysm is characterized by weakened mechanical integrity, direct injection of cells into the smooth muscle layer of the vessel wall is challenging and risks rupturing the aneurysm. On the other hand, systemic cell delivery severely limits cellular localization to the aneurysm site. As an alternative, biomaterials serve as an effective delivery vehicle for localizing the cells to the site of injury, while providing extracellular matrix (ECM) cues to support cell survival and function[12]. This has been demonstrated in several studies in the context of osteochondral regeneration, where cell-seeded scaffolds are already used in clinical settings[13,14]. To date, scaffold-based approaches for cell delivery to the site of AAA have been limited to only adipose-derived stromal cell therapy[15,16]. Accordingly, the therapeutic efficacy of scaffold-based SMC therapy for treatment of AAA remains largely unknown.

In this present study, we tested the efficacy of porous collagen scaffolds seeded with either primary human SMCs or iPSC-SMPs for treatment of experimental AAA in a murine model. Our findings demonstrate that this technique is feasible and highlights the potential of scaffold-based cell delivery as a therapeutic strategy for treatment of AAA.

2. Experimental

2.1 iPSC-SMP Differentiation

Primary adult human aortic SMCs (Invitrogen, passages 5-7) were cultured in Smooth Muscle Growth Medium (SMGM, Fisher Scientific), supplemented with recombinant human platelet-derived growth factor-BB (10 ng/mL, PDGF-BB; Sigma Aldrich). The human iPSC cell line (HUF5) was reprogrammed from dermal fibroblasts using viral vectors , and the smooth muscle phenotype of the iPSC-SMPs has been extensively characterized[17]. The human iPSC-SMPs were generated from our previously established differentiation protocol[10,18,19]. In brief, the iPSCs were cultured in a chemically defined medium consisting of RPMI 1640 with 1 mM Glutamax, 1% w/v

nonessential amino acids, 0.1 mM β-mercaptoethanol, 1% w/v insulin-transferrin-selenium supplemented with activin A (50 ng/mL), human bone morphogenetic protein 4 (BMP4, 50 ng/mL) and 2.5 μM/ml GSK 3 inhibitor CHIR99021 for two days, then following by supplementation with basic fibroblast growth factor (50 ng/mL) and vascular endothelial growth factor (40 ng/mL) for 10-12 days. The cells were then purified for vascular progenitor phenotype marker CD34 expression initially by magnetically activates cell sorting, followed by CD31+/CD34+ vascular progenitor expression by fluorescence activates cell sorting. The purified cells were expanded in vitro on mouse collagen IV coated plates in smooth muscle growth medium (SMGS) supplemented with PDGF-BB (10 ng/ml).

2.2 Comparative Analysis of Cellular Phenotype by Quantitative PCR

The cells were cultured on tissue culture dishes coated with 3% mouse collagen IV (Corning) for iPSC-SMPs and 0.1% gelatin for primary SMCs. Cells were seeded with an initial density of 2x105 cells per sample in the growth media (Medium231 with smooth muscle growth supplement, Fisher Scentific). To maintain their phenotype, PDGF-BB (10ng/mL) supplemented the growth medium for iPSC-SMPs. After 3-4 days when cells approximated 80% confluency, the media was switched to the differentiation media (Smooth Muscle Differentiation Media, Cell Applications), supplemented with 2.5 ng/ml transforming growth factor- β-1 (TGFβ-1) for 10 days. At the end of 10 days, the samples were lysed and processed for total RNA using the GeneJet RNA isolation kit (Fisher Scientific) according to the manufacturer's instructions. The total RNA was then transcribed into cDNA (Fisher Scientific) according to our previous methods[20]. Primers for qPCR consisted of ACTA2, TAGLN, CNN1, MYH11, COL1A, and GAPDH (Fisher Scientific). Relative fold change expression was normalized to GAPDH housekeeping gene using the ΔΔCT method, as described in our previous methods[21,22] and averaged out of n ≥3 samples per group.

2.3 Cell Seeding of Scaffolds

For cell seeding into scaffolds, iPSC-SMPs or primary aortic SMCs were dissociated using TrypLE (Fisher Scientific) and then seeded into Avitene™ Ultraform™ collagen sponges (Davol, 2.0 x 3.5 x 1.5 mm, L x W x D, pre-coated with 0.2% gelatin) at a density of ~5x10⁵ cells per scaffold. For non-invasive in vivo tracking, the cells within iPSC-SMP-seeded scaffolds were tagged by nucleofection of luciferase under a constitutively active promoter[11]. For a subset of primary SMC-seeded scaffolds, the SMCs were lentivirally transduced with a double fusion reporter consisting of the constitutively active promoter driving both luciferase and green fluorescence protein (GFP) [17,23]. For in vitro analysis, the cell-seeded scaffolds were grown in growth media for 24 hours before fixing in 4% paraformaldehyde. For in vivo studies, the cell-seeded scaffolds were grown in growth media for 24 hours before transplantation.

2.4 In-vitro Characterization of Cell-Seeded Scaffolds

At 24 hours following cell seeding into scaffolds in growth media, the samples underwent in vitro analysis of cell viability, cell penetrance into the scaffold, and preservation of smooth muscle phenotype. The cell-seeded scaffolds were incubated with fluorescent vital dyes from the Live/Dead Cytotoxicity Kit (Fisher Scientific) according to manufacturer's directions, and then immediately imaged using a fluorescence microscope (Keyence, BZ-X700) or a confocal microscope (Zeiss, LSM710). Confocal images were captured from the top and bottom faces of the scaffolds at intervals of ~8μm per image for up to 80μm thickness from the scaffold surface. To quantify the degree of cell viability, the number of viable cells from both

faces were counted and expressed as a percentage of total cells. To examine cell viability at varying depths through the scaffold, the percentage of viable cells was quantified at 0 µm, 25 µm, 50 µm, and 75 µm depths from the surface of the scaffold (n=3-6). After confocal imaging, the cell-seeded scaffolds were embedded into OCT for transverse cryosectioning. From the 10µm cross-sectional slices of the cell-seeded scaffolds, the cells were visualized by staining of Alexafluor 488-conjugated F-actin (Fisher Scientific) and Hoechst 33342 nuclear dye. The degree of cell penetration through the scaffold was quantified based on previous publications[24] by measuring the straight-line distance through the scaffold cross section that was occupied by cells using the Image J line measurement tool, and then expressing the data in the form of a percentage (n=3).

Additional samples were fluorescently stained for F-actin for cellular morphology or immunofluorescently stained for the smooth muscle phenotypic marker, smooth muscle α-actin (αSMA), based on our previous publications[18]. In brief, the samples were fixed in 4% paraformaldehyde, then permeabilized in 0.1% Triton-X-100, and then blocked in 0.1% bovine serum albumin. Primary antibody directed against smooth muscle α-actin (α-SMA, Sigma) was then applied to the samples, followed by the application of Alexafluor-488-conjugated anti-mouse antibody. For visualization of F-actin assembly, the samples were incubated with Alexafluor-488-conjugated phalloidin (Fisher Scientific). All samples were counterstained with Hoechst 3342 nuclear dye and then imaged using a Leica LSM710 confocal microscope at 10X magnification.

2.5 Proteomic analysis of inflammatory cytokines

Using the same cell-seeded samples for cell viability analysis, conditioned media was collected at 24 hours after cell seeding. Proteomic analysis of inflammatory-related cytokines was performed by the Immunoassay Team at the Human Immune Monitoring Center at Stanford University. An inflammation array (Milliplex HCYTA-60K-PX48) from EMD Millipore Corporation (Burlington, MA) was run according to the manufacturer's recommendations. In brief, supernatants samples were run without dilution. Samples were added to antibody-linked magnetic beads in a 96-well plate and incubated overnight at 4°C with shaking. Cold and room temperature incubation steps were performed on an orbital shaker (500-600 rpm). The plates were washed twice with phosphate buffered saline wash buffer in a Biotek ELx405 washer (BioTek Instruments, Winooski, VT). Following one-hour incubation at room temperature with biotinylated detection antibody, phycoerythrin-conjugated streptavidin was added for 30 minutes with shaking. The plates were washed again, and new wash buffer was added to wells for reading in the Luminex FlexMap3D Instrument with a lower bound of 50 beads per sample per cytokine. Reference control samples consisted of sample buffer or normal growth medium. Custom Assay Chex control beads were added to all wells (Radix Biosolutions, Georgetown, Texas). Wells with a bead count <50 were flagged, and data with a bead count <20 were excluded (n=3-6). Data is shown as a heat map depicting mean fold change.

2.6 Mechanical Characterization of Scaffolds

Mechanical characterization of Young's Modulus was performed based on our previous study[25]. Collagen scaffolds (10 mm × 5 mm × 2 mm) were clamped longitudinally on the Universal Testing Machine (Instron 5565). A constant strain was applied at 10 mm/min. Tensile force was measured by a 100 N load cell, and the test was concluded when each sample failed by tearing. Data output in the form of force-displacement curves were analyzed to produced stress-strain curves. The Young's modulus was calculated from the gradient of the elastic region of each stress-strain

curve. Maximum load was determined from the highest force measured in the force displacement curve (n=4).

2.7 Generation of Murine AAA Model and Scaffold Implantation

Murine models of AAA are commonly tested in immunocompetent strains of mice, such as the C57BL/6 strain, using a standard model of porcine pancreatic elastase infusion (PPE)[26–29]. We chose to perform the animal studies using the C57BL/6 strain because the PPE model in C57BL/6 mice is well-established and within our surgical expertise[26–29]. Despite the need for immunosuppressive therapy to obviate rejection of human cells, such a model better mimics the clinical application of allogenic human stem cell therapy, which requires immunosuppression. On day 0 of the study timeline, ten-week-old male C57BL/6 mice (Jackson Laboratory) were subjected to PPE infusion into the infrarenal abdominal aorta to induce aneurysm formation, as previously described. Elastase (2.5 U/ml) was infused for 5 minutes at 130 mmHg. Weekly ultrasound imaging (Vevo 2100®, VisualSonics) of aortic diameters was used to track aneurysm growth. The incidence of AAA formation was depicted by Kaplan Meier curves, in which AAA formation was defined as having greater than a 50% increase in abdominal aortic diameter, compared with the baseline diameter on day 0[30]. On day 7 following surgery, the laparotomy was re-opened to implant the cell-seeded scaffolds. To prevent detachment of the scaffold, a biocompatible thin film composed of polycaprolactone (PCL, 5x5mm) was placed on top of the scaffold and fixed to surrounding tissue with 10.0 sutures. Control animals received scaffolds of same size without cells, while a separate control cohort did not receive scaffold implantation following AAA induction. Except where noted, all animals received daily cyclosporine A (15 mg/kg) subcutaneous injections starting from day 5 after PPE induction to limit immune reaction to human cells. One additional cohort of control animals did not receive cyclosporine A, to evaluate its potential impact on AAA growth. All surgical and non-invasive procedures were performed in accordance with the Guidelines of Care and use of Laboratory Animals at the Veterans Affairs Palo Alto Health Care System and approved by the Institutional Animal Care and Use Committee.

2.8 Tracking of In Vivo Cell Localization and Survival by Bioluminescence Imaging (BLI)

After transplantation of the cell-seeded scaffold, *in vivo* bioluminescence imaging was performed to track the localization and number of viable implanted cells in the animals[23,31]. At selected timepoints from day 7 to day 28 post-PPE induction, the animals were injected intraperitoneally with D-firefly luciferin (159mg/kg) and imaged using the IVIS Spectrum *in vivo* imaging system (Perkin Elmer). Bioluminescence imaging data from each animal is shown as the average radiance ($p/cm^2/s/sr$).

2.9 Immunohistochemistry of Tissue Sections

On day 28 of the study timeline, murine abdominal aortas were harvested and processed using routine paraffin-embedding and tissue sectioning. Tissue sections were immunochemically stained with a rat anti-human F4/80 antibody (Abcam, 0.5 µg/ml) and a rabbit anti-CD206 antibody (Proteintech, 1.75 µg/ml) for assessment of macrophages. Additionally, immunohistochemistry was performed to evaluate smooth muscle cell retention in the smooth muscle layer by using a mouse anti-smooth muscle actin antibody (αSMA, Sigma-Aldrich, 26 µg/ml) or rabbit anti-calponin antibody (Abcam, 110 µg/ml). Immunohistochemistry was carried out using rat, mouse, or rabbit Vectastain ABC horseradish peroxidase kits according to the manufacturer's instructions. Positive areas in the aortic media were quantified (3 high power fields

(HPF) from 3 slides per animal, and among at least 3 animals per treatment group, using ImageJ's IHC toolbox plugin. Negative control samples consisted of samples in which primary antibodies were omitted. Additionally, to further visualize the presence of the remaining implanted primary SMCs, tissue sections derived from treatment of scaffolds seeded with primary SMCs were incubated with Alexa Fluor-488-conjugated anti-GFP antibody (Thermo Fisher, 20 µg/ml) and Hoechst 33342 (Life Technologies) before imaging using fluorescence microscopy (Keyence, BZ-X700).

2.10 Statistical Analysis

Unless otherwise noted, data are presented as mean ± standard error of the mean (SEM). The number of mice (n) is specified in the figure legends whenever data are not plotted as individual data points. For proteomic analysis, the fold change comparisons between two groups were performed by a Student's t-test. Comparisons with greater than two groups were performed by one-way ANOVA followed by Tukey's multiple comparisons test. Sequential measurements were analyzed by two-way ANOVA with multiple comparison. AAA incidence was compared using Kaplan-Meier analysis with subsequent log rank comparison. A fixed value of $p < 0.05$ was the criterion for reliable differences between groups, while non-significant comparisons are shown as "ns". All statistical analyses were performed using Prism 8 (GraphPad).

3. Results

3.1 In Vitro *Characterization of Porous Collagen Scaffolds Seeded with SMCs or iPSC-SMPs*

The phenotype of human iPSC-SMPs was first verified in comparison to primary human SMCs. Based on qPCR assessment of phenotypic smooth muscle markers, the iPSC-SMPs showed comparable levels of expression to primary SMCs for ACTA2, CNN1, TAGLN, and MYH11 (**Suppl. Fig. 1**). This data suggested that iPSC-SMPs were phenotypically similar to primary SMCs. Next, to determine the feasibility of delivering primary SMCs or iPSC-SMPs within biomimetic scaffolds, we performed *in vitro* assessment of cellular adhesion, penetration, morphology, and phenotype. We selected a commercially available three-dimensional sponge composed of porous microfibrillar collagen because of its safety and suitability for clinical use (**Fig. 1A**). Mechanical characterization demonstrated that the scaffold's Young's modulus was 1124 ± 47 kPa (n=4), which indicated high tensile strength of the material. Accordingly, the scaffolds were easy to handle and remained intact during cell-seeding as well as subsequent surgical implantation. The commercial scaffolds were subsequently trimmed to dimensions of 2.0 x 3.5 x 1.5 mm for subsequent *in vitro* and *in vivo* studies.

After the scaffolds were seeded with either human SMCs or human iPSC-SMPs for 24 hours, they were cryosectioned transversely to visualize the depth of cellular penetration. Based on F-actin staining of cell nuclei in the scaffold cross sections, both the SMCs and iPSC-SMPs were able to penetrate ~80% through the thickness of the scaffold (**Fig. 1B**). Additionally, the cell-seeded scaffolds were assessed for cytotoxicity and cell attachment using the Live/Dead Cytotoxicity Assay, in which viable cells take up calcein-AM (green) and non-viable cells become permeable to ethidium homodimer (red) (**Fig. 1C**). Fluorescent images suggested a high degree of cell viability (>75% viability) for both cell types at varying depths up to 80 µm into the scaffold (**Fig. 1D**). No statistical difference in cell viability was noted between cell types at any of the depths analyzed. To further verify the morphology and phenotype of the cells at 24 hours after seeding into collagen scaffolds, the samples were stained for F-actin and smooth muscle α-actin (αSMA). The elongated F-actin assembly suggested

that the cells were adherent to the scaffolds, and the abundant expression of αSMA suggested the maintenance of smooth muscle phenotype after cell seeding into collagen scaffolds (**Fig. 1E-H**). Together, these *in vitro* data suggested that both primary SMCs and iPSC-SMPs were viable, adherent in morphology, and retained their smooth muscle phenotype while being encapsulated within the porous scaffolds.
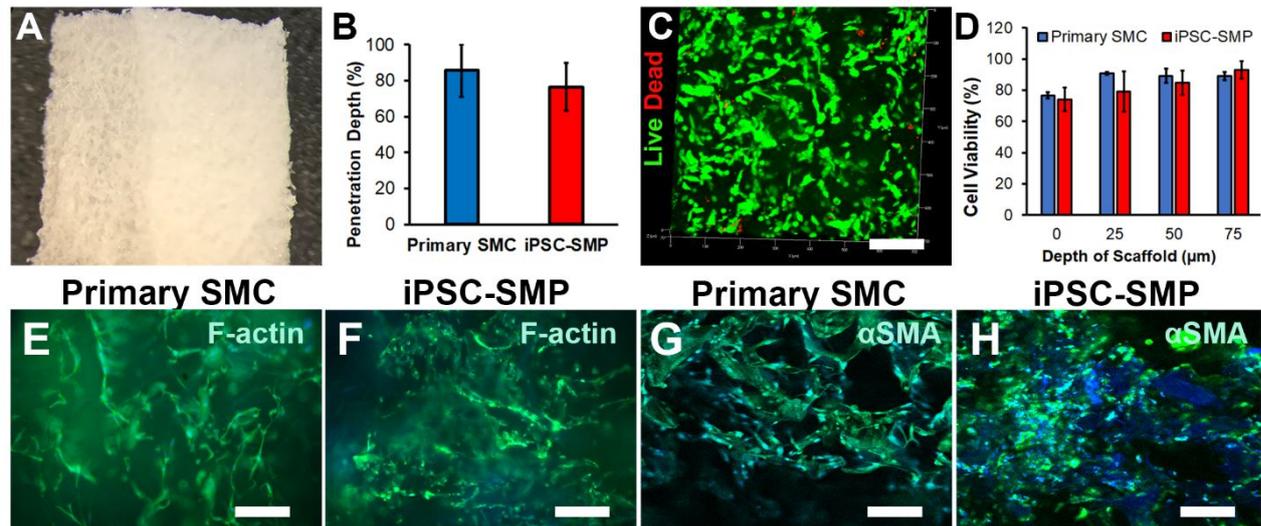

Figure 1. *In vitro* **characterization of human SMCs or iPSC-SMPs embedded within porous collagen scaffold for 24 hours. A.** Gross image of three-dimensional collagen scaffold. **B.** Quantification of cell penetration through the thickness of the scaffold, based on image analysis of scaffold cross sections fluorescently stained with F-actin (n=3). **C.** Representative three-dimensional reconstruction of scaffold-seeded iPSC-SMPs stained with the Live/Dead viability assay through an 80-μm-thick scaffold region. **D**. Quantification of cell viability at different depth levels of the scaffolds, as assessed by Live/Dead viability assay. **E-F.** Fluorescent staining of F-actin filaments using phalloidin (green) in scaffolds seeded with primary SMCs (**E**) or iPSC-SMPs (**F**). **G-H.** Immunofluorescent staining of α-smooth muscle actin (αSMA, green) in scaffolds seeded with primary SMCs (**G**) or iPSC-SMPs (**H**). Cell nuclei are counterstained with Hoechst (blue). Scale bar: 1 mm (A), 150 μm (C), 100 μm (E-H). Data shown as mean ± SEM.

3.2 Assessment of Abdominal Aortic Diameter after PPE Induction

After the cell-seeded scaffolds were characterized *in vitro*, we explored whether they can be applied to a developing aneurysmal lesion to test their therapeutic potential. AAA was induced by infusion of PPE into the infrarenal aorta of C57BL/6 mice (8-12 weeks old) on day 0 (**Fig. 2A**). After 7 days of recovery, the animals were randomized to receive peri-adventitial implants composed of cell-seeded scaffolds carrying either iPSC-SMPs, SMCs, or no cells (acellular scaffold) along with the placement of a protective membrane over the scaffold to secure them in place (**Figs. 2B-2E),** or no scaffold treatment. Since the focus of the proposed studies was not only to test this route of delivery, but also to evaluate the therapeutic potential of human cells for treatment of AAA in a preclinical model, daily cyclosporine treatment starting from day 5 through day 28 was necessary to obviate immune rejection of human cells in mice.
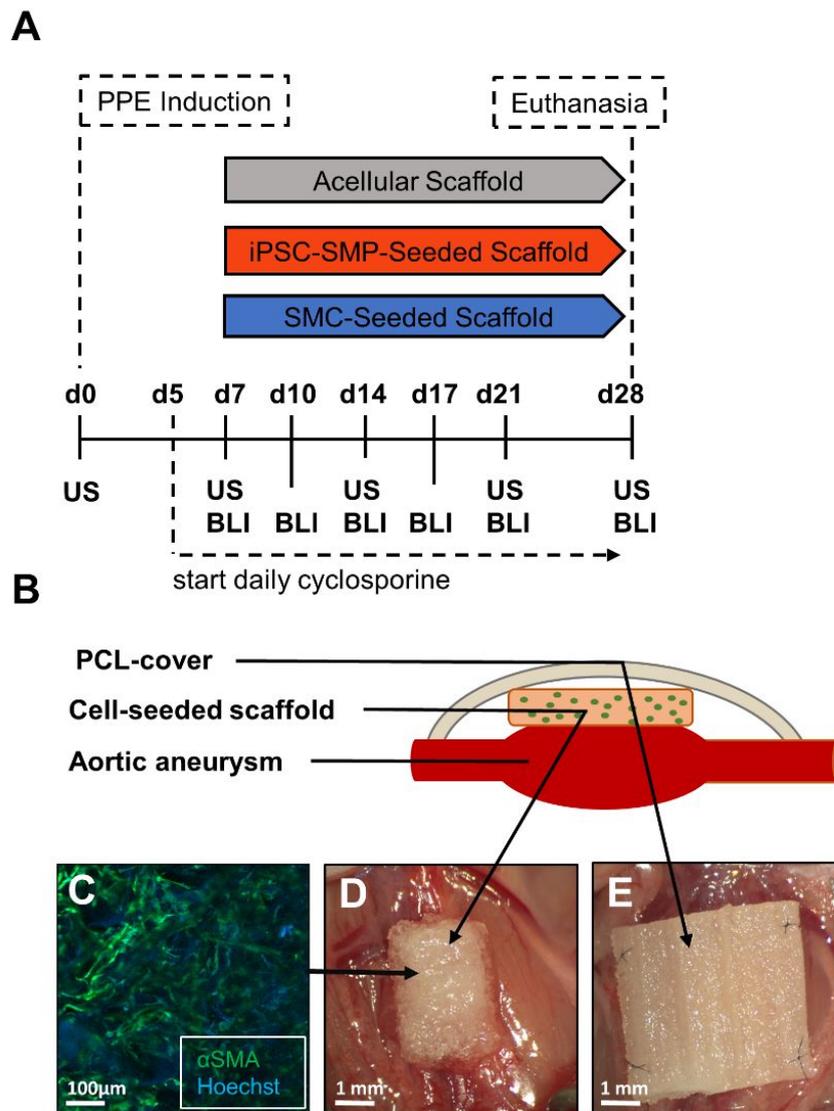
Figure 2. Schematic overview of cell-seeded scaffold transplantation onto the adventitia of the aneurysm in a murine model. A. Timeline of experiment design. Mice underwent porcine pancreatic elastase (PPE) infusion on day 0 to induce AAA formation. Daily cyclosporine-A injection was administered starting from day 0 to obviate immune rejection of human cells. Scaffolds were implanted on day 7. For up to day 28, abdominal aortic diameters were tracked using ultrasound (US), and transplant cell survival and localization were tracked by bioluminescence imaging (BLI). **B-E.** Schematic overview (**B**) and intraoperative (**C-E**) images of scaffold implantation procedure. Collagen scaffolds were seeded with either human iPSC-SMP, primary SMC (**C**), or no cells (acellular) and then implanted onto PPE-induced abdominal aneurysms on day 7 after PPE surgery (**D**). (**E**) A polycaprolactone (PCL) protective membrane was placed over the scaffold and fixed with sutures to the retroperitoneum to prevent adhesion and/or movement of the scaffold. Scale bars: 0.1 mm (C), 1 mm (D-E).
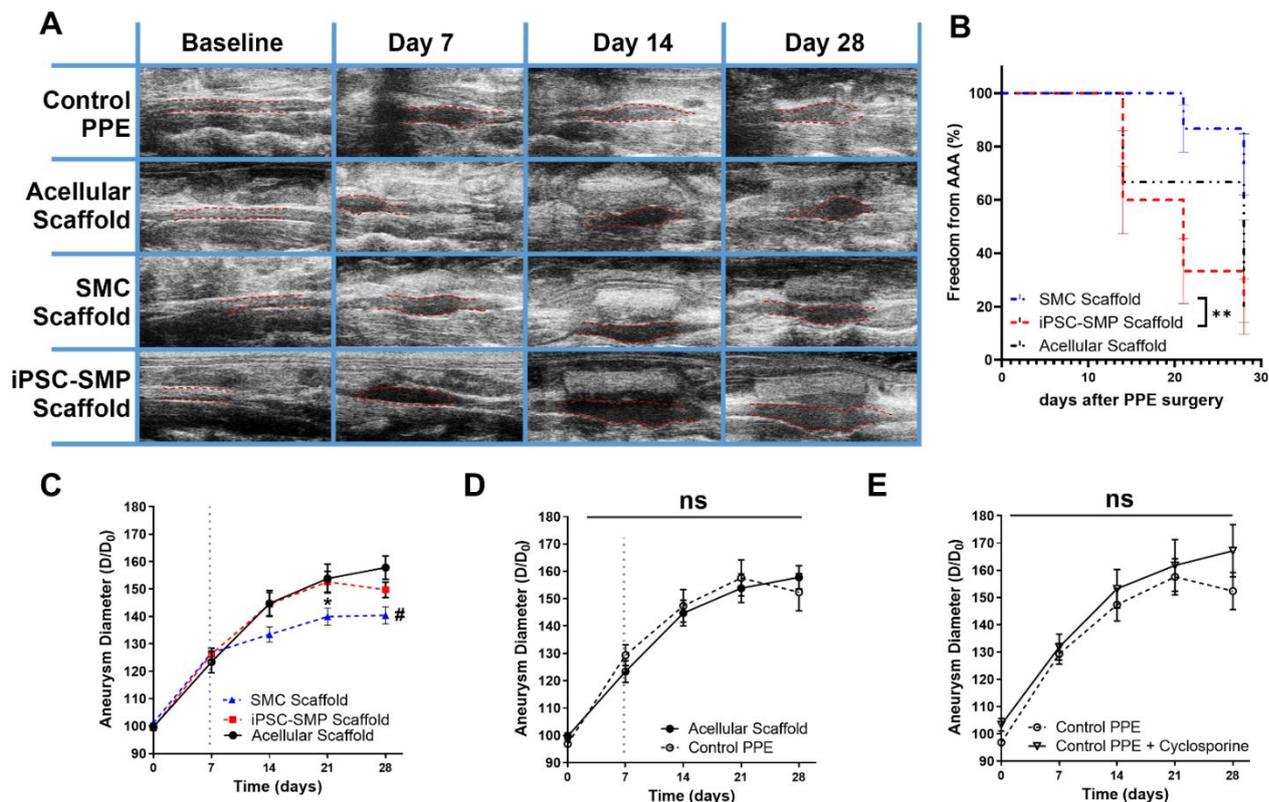
Figure 3. Therapeutic effect of transplanted cell-seeded scaffolds on aneurysm size. A. Representative ultrasound images from each treatment group over the course of 28 days. Dotted red lines show the outline of the aneurysm size. **B.** Kaplan Meier curves depict the Freedom of AAA (%), which is defined as the percentage of animals within each treatment group that remained free of aneurysm by being within 50% of the baseline aortic dimensions.** denotes statistically significant relationship when comparing treatment of iPSC-SMP-seeded scaffold (iPSC-SMP Scaffold) to primary SMC-seeded scaffold (Primary SMC Scaffold) on day 28 (p<0.01). **C.** Aortic diameter increase after PPE induction was measured by ultrasound on days after surgery as indicated. Data is presented as % increase vs. individual baseline diameter. Scaffolds were implanted on day seven (grey dotted line). * denotes statistically significant relationship comparing iPSC-SMP-seeded scaffold (n=15) to SMC-seeded scaffold (n=15) on day 21 (p<0.05); # denotes statistically significant relationship comparing Acellular scaffold (n=6) to SMC-seeded scaffold (n=15) on day 28 (p<0.05). **D.** No difference in growth rate was detected between PPE-treated mice undergoing scaffold implantation on day 7 and regular PPE surgery with no additional re-laparatomy (n= 6 per group). **E.** No significant difference in growth rate was detected in PPE-treated mice receiving cyclosporine (n=6) vs PPE only (control) (n= 6). Data shown as mean ± SEM.

For up to 28 days from the start of PPE induction, the abdominal aortic diameter was measured by ultrasound before and after PPE infusion to track AAA development. Protection from AAA development is associated with higher % freedom from AAA and decreased aneurysmal diameters. Compared to the acellular treatment group, mice treated with primary SMC-seeded scaffolds showed significantly less AAA development at day 28, based on significantly smaller aneurysm diameters (P<0.05) (**Fig. 3A-C**). Furthermore, the primary SMC-seeded scaffold group showed significantly decreased AAA growth, in comparison to the iPSC-SMC-seeded scaffold group on day 21 (P<0.05) (**Fig. 3C**). Additionally, the Freedom from AAA (%) was calculated as the percentage of animals in each treatment group whose abdominal aortic diameters showed less than a 50% increase in size, compared to baseline

measurements. As shown by the Kaplan Meier curves in **Fig. 3B**, 87% of the mice treated with SMC-seeded scaffolds were free from AAA for 28 days, which was significantly higher compared to 33% of mice treated with iPSC-SMP-seeded scaffolds (P<0.01). Furthermore, we determined that the implantation of the acellular scaffold alone did not significantly affect aneurysm expansion (**Fig. 3D**), which suggested that the cells played an important in modulating AAA expansion. Since the mice received daily immunosuppressive therapy of cyclosporine A to prevent cellular rejection, additional experiments were performed to compare the effect of aneurysm formation in the presence or absence of cyclosporine injection. Our results showed that cyclosporine injections did not affect AAA growth in the PPE model (**Fig. 3E**). Together, these studies demonstrated that only scaffolds seeded with primary SMCs could abrogate aneurysm expansion and had a higher percentage of freedom from AAA, compared to scaffolds seeded with iPSC-SMPs or to acellular scaffolds.

3.3 Tracking of In Vivo Cell Survival and Immunomodulation

In addition to assessing vessel size, we also tracked the numbers of viable SMCs and iPSC-SMPs, along with their localization, using bioluminescence imaging. As shown in **Fig. 4A-B**, both primary SMCs and iPSC-SMCs could be visualized soon after implantation in the abdominal cavity on day 7. However, by day 14 the cells from both treatment groups showed a pronounced reduction in bioluminescence signal, although the bioluminescence signal was higher in the iPSC-SMP than in the primary SMC group (**Fig. 4B**). By 28 days, the cellular retention in both groups reached a plateau of <10%, relative to the signal on day 7 (**Suppl. Fig. 2A**).
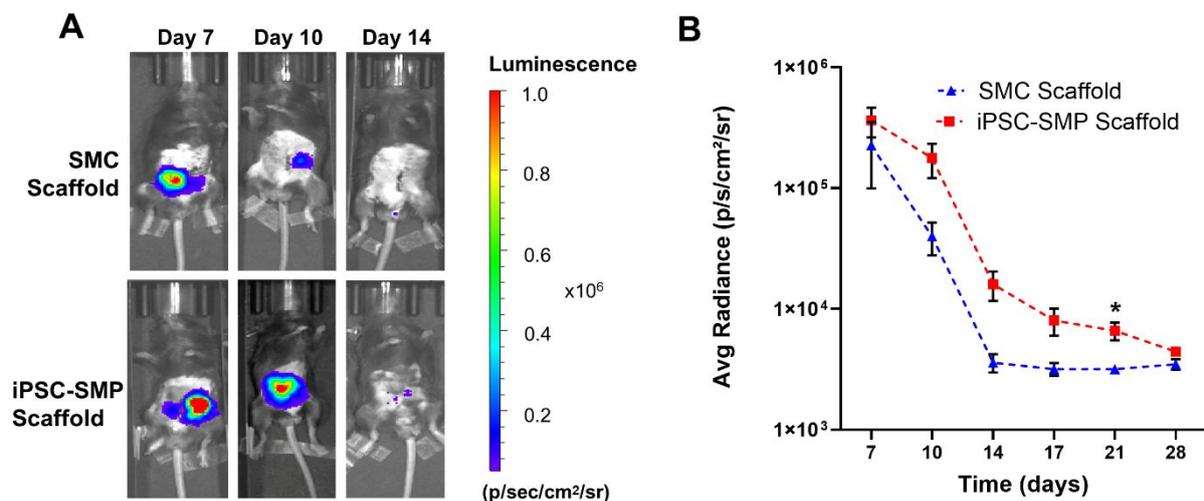

Figure 4. Cellular localization and survival *in vivo*. A. Representative images depicting the localization and survival of SMCs or iPSC-SMPs after transplantation to the site of AAA within scaffolds. **B.** Quantification of cell survival by bioluminescence imaging (n=5 for SMC; n=15 for iPSC-SMP). * denotes p<0.05 based on a Student's t-test. Data shown as mean ± SEM.

Since *in vivo* bioluminescence imaging has limited sensitivity to detect accurate cell numbers less than ~10^3-10^4 cells [32], we sought to visualize the presence and localization of any remaining primary SMCs within the scaffolds after explantation from animals on day 28. To visualize the presence of any remaining SMCs, we took advantage of the SMCs having a GFP tag and examined their location by fluorescence

microscopy. The GFP-labeled primary SMCs could be detected in the adventitia, with some of the cells having the appearance of being in proximity to the medial layer of the aneurysmal vessel wall. This data suggested that some of the transplanted cells remained viable were able to migrate to some extent towards the aortic wall from the adventitia **(Suppl. Fig. 2B)**.

Despite the gradual decline in cell survival over time, we assessed whether the transplanted cells could have had lasting impacts in regulating the inflammatory environment of the aneurysm, since inflammation is a major feature of AAA pathology. To determine whether the implantation of the collagen scaffold led to an augmented inflammatory response, we performed histological quantification of macrophages using antibodies targeting F4/80 or CD206. We quantified the positive areas within the media of AAA tissues to evaluate macrophage infiltration **(Fig. 5A-D)**. Lesions in the iPSC-SMP- and SMC-seeded scaffold group showed significantly less positive area when compared to acellular scaffold groups **(Fig. 5B, D)**. Our data suggest that the primary SMCs or iPSC-SMPs within the scaffolds may attenuate infiltration of macrophages into the vessel media. To further examine the potential immunomodulatory effects of these cells, we performed proteomic analysis of pro-inflammatory and anti-inflammatory related cytokines from cell-seeded scaffolds *in vitro*. Proteomic analysis demonstrated that, for most pro-inflammatory as well as anti-inflammatory cytokines, the primary SMCs showed higher fold change increases in abundance, compared to iPSC-SMPs (**Suppl. Fig. 3**). The fact that the iPSC-SMPs secreted globally much lower levels of cytokines than primary SMCs suggests that the iPSC-SMPs were not as immunologically active or functional.

We also sought to evaluate the retention of native SMCs in the tissue media using immunochemistry. Although we observed non-significant trends towards increased α-SMA-positive area when compared to acellular scaffold-treated animals (**Fig. 5E-H**), we saw significantly greater areas that were positive for SMC marker calponin (**Fig. 5F, H**). This finding suggests that both primary SMC- and iPSC-SMP-seeded scaffolds may help to promote native smooth muscle retention in the vessel media.
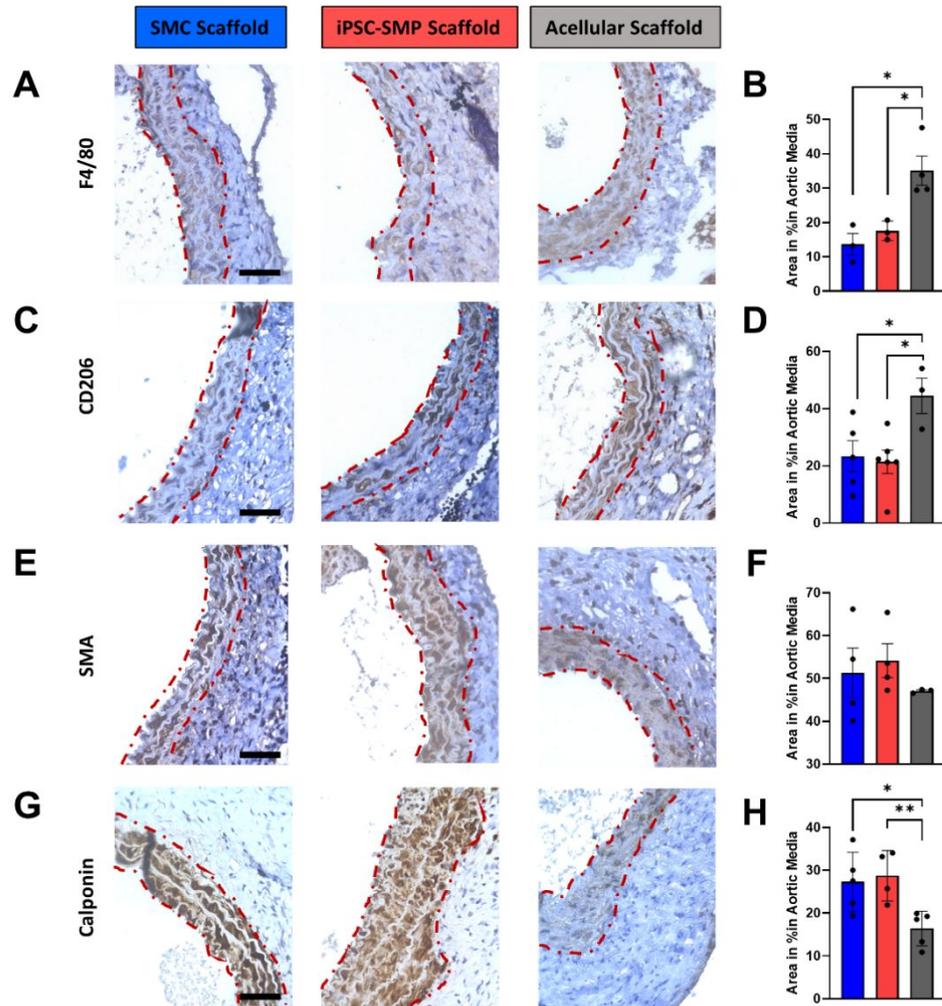
Figure 5. Histological assessment of vascular remodeling in the aneurysm after treatment of cell-seeded scaffolds. **A-B.** Representative images depicting immunohistochemical staining of general macrophage marker, F4/80 (**A**) and the corresponding quantification of F4/80 expression in the aneurysm media (**B**), as expressed as an area percentage. **C-D** Representative images depicting immunohistochemical staining of anti-inflammatory macrophage marker, CD206 (**C**) and the corresponding quantification of CD206 expression in the aneurysm media (**D**), as expressed as an area percentage. **E-H.** Representative images depicting immunohistochemical staining of general smooth muscle phenotypic markers, α-SMA (**E**) and calponin (**G**) and their corresponding graphs depicting area percentage in the aneurysm media (**F, H**).   All tissue samples were analyzed on day 28. Scale bar is 50 µm. Quantification was performed in 3 high power fields (HPF) (100x) of 3 different sections from 3 to 5 different animals per treatment group using ImageJ software. Data shown as mean ± SEM. Statistically significant relationships are denoted as *$p<0.05$ and **$p<0.01$.

4. Discussion

In this study, we evaluated whether cell-seeded collagen scaffolds can be applied to developing experimental AAA lesions in mice. Additionally, we tested if this route of delivery can be used to deliver human cells to evaluate the potential for future translational studies. Our results suggest that peri-adventitial delivery of scaffolds seeded with primary SMCs is feasible and can abrogate aneurysmal expansion (**Fig. 3B-C**). Although our data indicate cell survival for both subtypes up to 14 days after

cell delivery, we only observed attenuated AAA formation in mice treated with primary SMC-seeded scaffolds. Notably, growth attenuation curves began to separate by day 14 (**Fig. 3C**), and differences became progressively more significant in comparison to acellular scaffold at subsequent time points, despite the decrease in transplanted cell survival (**Fig. 4B**). Further, histological analysis demonstrated that both primary SMC- as well as iPSC-SMP-seeded scaffolds could attenuate macrophage infiltration into the aneurysmal wall, when compared to treatment with acellular scaffolds alone. Both cell-seeded scaffold groups promoted the retention of native smooth muscle cells in the vessel media. However, despite these histological findings that iPSC-SMP-seeded scaffolds attenuated macrophage infiltration and retention of smooth muscle cells, this treatment did not lead to improvements in aneurysmal expansion, which suggests a limited benefit of iPSC-SMP-seed scaffolds (**Fig. 3C**).

We also examined the potential immunodulatory effects of SMCs histologically by examining macrophage infiltration. We observed smaller F4/80 and CD206 positive areas in AAA treated with scaffolds seeded with primary SMC or iPSC-SMP, when compared to acellular seeded scaffolds. SMC are known to release macrophage-attracting factors such as tumor necrosis factor alpha or interleukin-6[33,34], but embedding in scaffolds, might alter the cytokine release profile[35]. As macrophages contribute to AAA progression by various cell-cell interactions and by releasing pro-inflammatory factors and proteases[36–38], less accumulation in the primary SMC- or iPSC-SMP-seeded scaffold treatment groups might have contributed to better outcomes.

We demonstrated the survival of both iPSC-SMP and primary SMC over a timeframe that would permit cell-cell interaction and migration into the layers of the vessel. Notably, *in vivo* BLI measurements have a detection limit of 10^3-10^4 cells[32]. Although cell signal in BLI imaging did decline over time, it is possible that there could have been sufficient surviving cells to alter functional outcome. This is supported by numerous examples of transplanted cells having limited engraftment or transient survival, but yet are able to impart significant therapeutic benefits in the cardiovascular system[39–42]. Another potential explanation is that the PPE model consist of an acute injury to the vessel with a strong inflammatory response in the first two weeks following surgery. The application of cells that have not been stimulated in the pro-inflammatory environment during that phase may have helped to attenuate the inflammatory response, which subsequently led to the reduced infiltration of macrophages as observed with both cell treatments. Future studies are warranted to investigate the potential mechanism of action of SMC-seeded scaffolds, which could include replacing the native SMCs or contributing to ECM remodeling[43]. Additional future studies include comparing the efficacy of scaffolds seeded with iPSC-SMPs to those seeded with terminally differentiated iPSC-derived SMCs, in order to reveal insights into the relationship between cellular maturation and therapeutic benefit.

Although both cell types abrogated macrophage infiltration and seemingly promoted native smooth muscle retention (**Fig. 5**), only the scaffolds seeded with primary SMCs ameliorated the expansion of the abdominal aorta (**Fig. 3A-C**). Given that this study was primarily designed to test the feasibility of human-derived, scaffold-based cell delivery, detailed exploration of mechanisms, which might have contributed to the observed effects, will be the subject to future experiments. The finding that only primary SMC-seeded scaffolds significantly reduced aneurysm expansion suggests that these cells might have a distinctive proteomic or transcriptional signature, compared to iPSC-SMPs. This is supported by our results from an exploratory Luminex based proteomic analysis of inflammatory cytokines (**Suppl. Fig. 3**), which revealed much lower overall expression of cytokines secreted by iPSC-SMPs. This indicates that primary SMCs

may have been more biological active and secreted more factors to interfere with macrophage activation and subsequent AAA progression. Future work is warranted to identify differences between these cell types through transcriptional and proteomic profiling approaches. To our knowledge this is the first study to compare the effects of primary SMCs to iPSC-SMPs as therapeutic cell types for treatment of AAA in a murine PPE model.

In contrast to the present study, a recent publication by Parvizi and colleagues reported success using a peri-adventitial collagen-based patch to deliver adipose tissue-derived stromal cells to rat aortas. The authors utilized an experimental model of AAA model which included combining PPE infusion with added topical calcium chloride[15]. In that study they seeded 2×10^6 cells on $1\ cm^2$ patches, while we used 5×10^5 cells per 2.0 x 3.5mm scaffold, which could partially explain differences from the effects seen in our study. Another interesting study by Park and colleagues evaluated stem cell delivery in a rat PPE model. The investigators first differentiated stem cells derived from rat skeletal muscle into vascular SMC-like progenitors, and then delivered the cells into the aortic lumen immediately after enzymatic wall degradation. They found that the vascular SMC-like progenitor cells attenuated AAA progression, in part by modulating matrix metalloproteinases. Despite these encouraging results, the clinical scalability and translatability of this cell type is unknown[44].

Based on these publications, additional pre-conditioning applied to both the cell types used and the scaffold could help to maximize cell survival and positive effects. A recent study by Ould-Brahim et al. showed that preconditioning of iPSC-derived neural stem cells led to improved outcomes in their animal model[45]. In the context of vascular SMCs, pre-conditioning could involve transforming growth factor-β treatment, which is crucial to SMC secretory and proliferative function[46]. Another approach of delivering cells was presented by Blose et al. who used a subcutaneous port to deliver adipose-derived MSCs in the murine PPE model of AAA[16], which would also allow repeated cell deliveries without the need for additional surgery.

To date, most cell-based methods to treat AAA involve the delivery of MSCs. Although some studies report successful intravenous delivery of MSC to attenuate murine experimental AAA formation, it remains controversial as to what extent these cells fulfill their regenerative potential at the site of injury[47,48]. For example, Hashizume et al. demonstrated that transplantation of MSCs onto the aortic adventitia could slow AAA progression in ApoE-/- mice receiving angiotensin-II infusion[49]. Although promising, MSCs as a regenerative source are viewed critically given their limited availability and potential ethical concerns[50]. Furthermore, the ability of MSCs to differentiate into contractile smooth muscle-like cells is unclear. Given these limitations, the present study utilized iPSC-SMPs as an alternative therapeutic stem cell.

One limitation of our study is that we imposed a regime of daily cyclosporine A injections to avoid rejection of implanted human cells following the implantation[51,52]. Although we did not observe notable changes in AAA diameters in response to cyclosporine (**Fig. 3E**), it is possible that cyclosporine A could have had other influences on the progression of AAA or on the therapeutic effect of cell-seeded scaffolds in vivo, which is documented in studies using other murine experimental models for AAA[53,54]. Given that the extend of the vascular injury is very localized, systemic anti-inflammatory effects of cyclosporine A might not be notable in the PPE model used in this study. Although similar studies could be performed using murine SMCs and iPSC-SMPs to obviate immune rejection, there could be species differences in the efficacy of therapeutic cells. With clinical translation in mind, we therefore focused on the use of human cells, necessitating the administration of cyclosporine A.

Another limitation is that we were not able to distinguish, whether increased positive staining for SMC markers after scaffold treatments was due to increased murine or human cell infiltration. Both interpretations, either through direct migration of human cells or paracrine effects upon murine cells, are possible. Future studies will be performed need to make such distinction.

For future studies, evaluation should be performed of transplanted SMC phenotype within the aortic wall and effects on proteinase activity and inflammatory signaling. Also, given that the scaffolds are transplanted onto the adventitia, it might be promising to deliver fibroblasts to promote adventitial remodeling. Optimizing the scaffold material to match mechanical properties of native aorta may help to minimize unwanted stiffening of the aortic wall, as differences of segmental stiffness have been shown to promote AAA formation[55]. In this regard, the implementation of scaffolds derived from elastin-like hydrogels may also help to replenish the loss of elastin which is part of AAA pathogenesis[56,57].

We believe that this technique holds the potential for translational approaches, as cell-seeded materials could be applied to human AAA lesions via minimal-invasive techniques to slow disease progression. Here, a minimally invasive, localized delivery of cells embedded within a material capable of providing transient mechanical support to the weakened AAA could change strategies for AAA treatment, also considering early-stage lesions. Additionally, cell-seeded elements could be added to endovascular devices to reduce for example the formation of endoleaks.

In conclusion, we report the therapeutic efficacy of delivering therapeutic SMCs in biocompatible scaffolds to attenuate experimental aortic aneurysm. Our approach has potential for translational AAA therapy, using scaffolds seeded with in-vitro expanded cells. Future validation of underlying molecular mechanisms and addressing of practical considerations are required to further develop this approach for potential use in patients.

at the Stanford Nano Shared Facilities (SNSF), which is supported by the National Science Foundation (ECCS-1542152).

Institutional Review Board Statement: All surgical and non-invasive procedures were performed according to protocols approved by the Institutional Animal Care and Use Committee at the Veterans Affairs Palo Alto Health Care System, as well as both the National Institutes of Health and U.S. Department of Agriculture Guidelines for Care and Use of Animals in Research.

Informed Consent Statement: Not applicable.

Data Availability Statement: All data from this project is available from the corresponding author upon reasonable request.

Conflicts of Interest: The authors declare no conflict of interest. The funders had no role in the design of the study; in the collection, analyses, or interpretation of data; in the writing of the manuscript, or in the decision to publish the results.

References

1   A. T. Hirsch, Z. J. Haskal, N. R. Hertzer, C. W. Bakal, M. A. Creager, J. L. Halperin, L. F. Hiratzka, W. R. C. C. Murphy, J. W. Olin, J. B. Puschett, K. A. Rosenfield, D. Sacks, J. C. Stanley, L. M. Taylor, C. J. White, J. White, R. A. White, E. M. Antman, S. C. Smith, C. D. Adams, J. L. Anderson, D. P. Faxon, V. Fuster, R. J. Gibbons, S. A. Hunt, A. K. Jacobs, R. Nishimura, J. P. Ornato, R. L. Page, B. Riegel, American Association for Vascular Surgery, Society for Vascular Surgery, Society for Cardiovascular Angiography and Interventions, Society for Vascular Medicine and Biology, Society of Interventional Radiology, ACC/AHA Task Force on Practice Guidelines Writing Committee to Develop Guidelines for the Management of Patients With Peripheral Arterial Disease, American Association of Cardiovascular and Pulmonary Rehabilitation, National Heart, Lung, and Blood Institute, Society for Vascular Nursing, TransAtlantic Inter-Society Consensus and Vascular Disease Foundation, *Circulation*, 2006, **113**, e463–e465.

2   E. J. Benjamin, S. S. Virani, C. W. Callaway, A. M. Chamberlain, A. R. Chang, S. Cheng, S. E. Chiuve, M. Cushman, F. N. Delling, R. Deo, S. D. De Ferranti, J. F. Ferguson, M. Fornage, C. Gillespie, C. R. Isasi, M. C. Jiménez, L. C. Jordan, S. E. Judd, D. Lackland, J. H. Lichtman, L. Lisabeth, S. Liu, C. T. Longenecker, P. L. Lutsey, J. S. MacKey, D. B. Matchar, K. Matsushita, M. E. Mussolino, K. Nasir, M. O'Flaherty, L. P. Palaniappan, A. Pandey, D. K. Pandey, M. J. Reeves, M. D. Ritchey, C. J. Rodriguez, G. A. Roth, W. D. Rosamond, U. K. A. Sampson, G. M. Satou, S. H. Shah, N. L. Spartano, D. L. Tirschwell, C. W. Tsao, J. H. Voeks, J. Z. Willey, J. T. Wilkins, J. H. Y. Wu, H. M. Alger, S. S. Wong and P. Muntner, *Circulation*, 2018, **137**, E67–E492.

3   E. L. Chaikof, R. L. Dalman, M. K. Eskandari, B. M. Jackson, W. A. Lee, M. A. Mansour, T. M. Mastracci, M. Mell, M. H. Murad, L. L. Nguyen, G. S. Oderich, M. S. Patel, M. L. Schermerhorn and B. W. Starnes, *J. Vasc. Surg.*, 2018, **67**, 2-77.e2.

4   J. B. J.-B. Michel, G. Jondeau and Di. M. M. Milewicz, *Cardiovasc. Res.*, 2018, **114**, 578–589.

5 E. L. Henderson, Y. J. Geng, G. K. Sukhova, A. D. Whittemore, J. Knox and P. Libby, *Circulation*, 1999, **99**, 96–104.

6 E. Allaire, B. Muscatelli-Groux, C. Mandet, A.-M. Guinault, P. Bruneval, P. Desgranges, A. Clowes, D. Méllière and J.-P. Becquemin, *J. Vasc. Surg.*, 2002, **36**, 1018–26.

7 C. L. Lino Cardenas, C. W. Kessinger, C. MacDonald, A. S. Jassar, E. M. Isselbacher, F. A. Jaffer and M. E. Lindsay, *JCI insight*, , DOI:10.1172/jci.insight.97493.

8 F. Schneider, F. Saucy, R. de Blic, J. Dai, F. Mohand, H. Rouard, J.-B. J.-B. Ricco, J.-P. J.-P. Becquemin, M. Gervais and E. Allaire, *Eur. J. Vasc. Endovasc. Surg.*, 2013, **45**, 666–72.

9 E. M. Maguire, Q. Xiao and Q. Xu, *Arterioscler. Thromb. Vasc. Biol.*, 2017, **37**, 2026–2037.

10 Y. Zhou, G. Kang, Y. Wen, M. Briggs, V. Sebastiano, R. Pederson and B. Chen, *Stem Cells Dev.*, 2018, **27**, 1438–1448.

11 Y. Li, Y. Wen, Z. Wang, Y. Wei, P. Wani, M. Green, G. Swaminathan, A. Ramamurthi, R. R. Pera and B. Chen, *Stem Cells Transl. Med.*, 2016, **5**, 1719–1729.

12 N. F. Huang, R. J. Lee and S. Li, *Tissue Eng.*, 2007, 13, 1809–1823.

13 N. Ma, H. Wang, X. Xu, Y. Wan, Y. Liu, M. Wang, W. Yu, Y. Dai, J. Peng, Q. Guo, C. Yu and S. Lu, *Trials*, , DOI:10.1186/s13063-017-2251-6.

14 S. Jiang, W. Guo, G. Tian, X. Luo, L. Peng, S. Liu, X. Sui, Q. Guo and X. Li, *Stem Cells Int.*, 2020, 2020.

15 M. Parvizi, A. H. Petersen, C. A. F. M. van Spreuwel-Goossens, S. G. J. M. Kluijtmans and M. C. Harmsen, *J. Biomed. Mater. Res. Part A*, 2018, **106**, 2494–2506.

16 K. J. Blose, T. L. Ennis, B. Arif, J. S. Weinbaum, J. A. Curci and D. A. Vorp, *Regen. Med.*, 2014, **9**, 733–41.

17 A. J. Rufaihah, N. F. Huang, S. Jamé, J. C. Lee, H. N. Nguyen, B. Byers, A. De, J. Okogbaa, M. Rollins, R. Reijo-Pera, S. S. Gambhir and J. P. Cooke, *Arterioscler. Thromb. Vasc. Biol.*, 2011, **31**, e72-9.

18 K. H. Nakayama, P. A. Joshi, E. S. Lai, P. Gujar, L. M. Joubert, B. Chen and N. F. Huang, *Regen. Med.*, 2015, **10**, 745–755.

19 Y. Li, M. Green, Y. Wen, Y. Wei, P. Wani, Z. Wang, R. Reijo Pera and B. Chen, *Stem Cells Transl. Med.*, 2017, **6**, 1158–1167.

20 K. H. Nakayama, M. Quarta, P. Paine, C. Alcazar, I. Karakikes, V. Garcia, O. J. Abilez, N. S. Calvo, C. S. Simmons, T. A. Rando and N. F. Huang, *Commun. Biol.*, 2019, **2**, 170–170.

21   N. F. Huang, F. Fleissner, J. Sun and J. P. Cooke, *Stem Cells Dev.*, 2010, **19**, 1617–1625.

22   M. Wanjare, L. Hou, K. H. Nakayama, J. J. Kim, N. P. Mezak, O. J. Abilez, E. Tzatzalos, J. C. Wu and N. F. Huang, *Biomater. Sci.*, 2017, **5**, 1567–1578.

23   N. F. Huang, J. Okogbaa, A. Babakhanyan and J. P. Cooke, *Theranostics*, 2012, 2, 346–354.

24   J. J. Kim, L. Hou, G. Yang, N. P. Mezak, M. Wanjare, L. M. Joubert and N. F. Huang, *Cell. Mol. Bioeng.*, 2017, **10**, 417–432.

25   K. H. Nakayama, C. Alcazar, G. Yang, M. Quarta, P. Paine, L. Doan, A. Davies, T. A. Rando and N. F. Huang, *npj Regen. Med.*, , DOI:10.1038/s41536-018-0054-3.

26   L. Maegdefessel, J. Azuma, R. Toh, A. Deng, D. R. Merk, A. Raiesdana, N. J. Leeper, U. Raaz, A. M. Schoelmerich, M. V McConnell, R. L. Dalman, J. M. Spin and P. S. Tsao, *Sci. Transl. Med.*, 2012, **4**, 122ra22.

27   L. Maegdefessel, J. Azuma and P. S. Tsao, *Trends Cardiovasc. Med.*, 2014, **24**, 1–6.

28   L. Maegdefessel, J. M. Spin, U. Raaz, S. M. Eken, R. Toh, J. Azuma, M. Adam, F. Nakagami, F. Nagakami, H. M. Heymann, E. Chernogubova, E. Chernugobova, H. Jin, J. Roy, R. Hultgren, K. Caidahl, S. Schrepfer, A. Hamsten, P. Eriksson, M. V McConnell, R. L. Dalman and P. S. Tsao, *Nat. Commun.*, 2014, **5**, 5214.

29   J. Mulorz, J. M. Spin, H. C. Beck, M. L. Tha Thi, M. U. Wagenhäuser, L. M. Rasmussen, J. S. Lindholt, P. S. C. Tsao, L. B. Steffensen, P. S. Chung Tsao and L. B. Steffensen, *Atherosclerosis*, 2020, **311**, 73–83.

30   W. Wang, B. Xu, H. Xuan, Y. Ge, Y. Wang, L. Wang, J. Huang, W. Fu, S. A. Michie and R. L. Dalman, *J. Vasc. Surg.*, 2018, **68**, 1538-1550.e2.

31   A. A. Foster, R. E. Dewi, L. Cai, L. Hou, Z. Strassberg, C. A. Alcazar, S. C. Heilshorn and N. F. Huang, *Biomater. Sci.*, 2018, **6**, 614–622.

32   A. Y. Sheikh, S.-A. Lin, F. Cao, Y. Cao, K. E. A. van der Bogt, P. Chu, C.-P. Chang, C. H. Contag, R. C. Robbins and J. C. Wu, *Stem Cells*, 2007, **25**, 2677–2684.

33   D. Ramel, S. Gayral, M.-K. Sarthou, N. Augé, A. Nègre-Salvayre and M. Laffargue, *Front. Pharmacol.*, 2019, **10**, 1276.

34   E. Butoi, A. M. Gan, M. M. Tucureanu, D. Stan, R. D. Macarie, C. Constantinescu, M. Calin, M. Simionescu and I. Manduteanu, *Biochim. Biophys. Acta*, 2016, **1863**, 1568–78.

35   J. Qiu, Y. Zheng, J. Hu, D. Liao, H. Gregersen, X. Deng, Y. Fan and G. Wang, *J. R. Soc. Interface*, 2014, **11**, 20130852.

36   K. Shimizu, R. N. Mitchell and P. Libby, *Arterioscler. Thromb. Vasc. Biol.*, 2006, **26**, 987–994.

37   J. Raffort, F. Lareyre, M. Clément, R. Hassen-Khodja, G. Chinetti and Z. Mallat, *Nat. Rev. Cardiol.*, 2017, **14**, 457–471.

38   M. A. Dale, M. K. Ruhlman and B. T. Baxter, *Arterioscler. Thromb. Vasc. Biol.*, 2015, **35**, 1746–1755.

39   L. M. McGinley, J. McMahon, A. Stocca, A. Duffy, A. Flynn, D. O'Toole and T. O'Brien, *Hum. Gene Ther.*, 2013, **24**, 840–851.

40   M. F. Berry, A. J. Engler, Y. J. Woo, T. J. Pirolli, L. T. Bish, V. Jayasankar, K. J. Morine, T. J. Gardner, D. E. Discher and H. L. Sweeney, *Am. J. Physiol. - Hear. Circ. Physiol.*, , DOI:10.1152/ajpheart.01017.2005.

41   D. Zhu, P. Wu, C. Xiao, W. Hu, T. Zhang, X. Hu, W. Chen and J. Wang, *Front. Cell Dev. Biol.*, , DOI:10.3389/fcell.2020.583700.

42   C. Toma, M. F. Pittenger, K. S. Cahill, B. J. Byrne and P. D. Kessler, *Circulation*, 2002, **105**, 93–98.

43   H. Ji, H. S. Kim, H.-W. Kim and K. W. Leong, *Curr. Opin. Biomed. Eng.*, 2017, **1**, 38–44.

44   H. S. Park, G. H. Choi, S. Hahn, Y. S. Yoo, J. Y. Lee and T. Lee, *Biochem. Biophys. Res. Commun.*, 2013, **431**, 326–331.

45   F. Ould-Brahim, S. N. Sarma, C. Syal, K. J. Lu, M. Seegobin, A. Carter, M. S. Jeffers, C. Doré, W. L. Stanford, D. Corbett and J. Wang, *Stem Cells Dev.*, 2018, **27**, 1085–1096.

46   P. A. Suwanabol, S. M. Seedial, X. Shi, F. Zhang, D. Yamanouchi, D. Roenneburg, B. Liu and K. C. Kent, *J. Vasc. Surg.*, 2012, **56**, 446–54.

47   X. Fu, A. Yamawaki-Ogata, H. Oshima, Y. Ueda, A. Usui and Y. Narita, *J. Transl. Med.*, 2013, **11**, 175.

48   J. P. Davis, M. Salmon, N. H. Pope, G. Lu, G. Su, A. K. Sharma, G. Ailawadi and G. R. Upchurch, *J. Surg. Res.*, 2015, **199**, 249–58.

49   R. Hashizume, A. Yamawaki-Ogata, Y. Ueda, W. R. Wagner and Y. Narita, *J. Vasc. Surg.*, 2011, **54**, 1743–52.

50   B. Lukomska, L. Stanaszek, E. Zuba-Surma, P. Legosz, S. Sarzynska and K. Drela, *Stem Cells Int.*, 2019, **2019**, 9628536.

51   N. Sachewsky, J. Hunt, M. J. Cooke, A. Azimi, T. Zarin, C. Miu, M. S. Shoichet and C. M. Morshead, *Dis. Model. Mech.*, 2014, **7**, 953–61.

52   Z. Xiao, J. Shan, C. Li, L. Luo, J. Lu, S. Li, D. Long and Y. Li, *Am. J. Nephrol.*, 2013, **37**, 30–40.

53   V. Esteban, N. Méndez-Barbero, L. J. Jiménez-Borreguero, M. Roqué, L. Novensá, A. B. García-Redondo, M. Salaices, L. Vila, M. L. Arbonés, M. R. Campanero and J. M. Redondo, *J. Exp. Med.*, 2011, **208**, 2125–2139.

54   J. Dai, S. Michineau, G. Franck, P. Desgranges, J.-P. Becquemin, M. Gervais and E. Allaire, *PLoS One*, 2011, **6**, e28903.

55   U. Raaz, A. M. Zöllner, I. N. Schellinger, R. Toh, F. Nakagami, M. Brandt, F. C. Emrich, Y. Kayama, S. Eken, M. Adam, L. Maegdefessel, T. Hertel, A. Deng, A. Jagger, M. Buerke, R. L. Dalman, J. M. Spin, E. Kuhl and P. S. Tsao, *Circulation*, 2015, **131**, 1783–95.

56   F. Cipriani, B. Ariño Palao, I. Gonzalez De Torre, A. Vega Castrillo, H. J. Aguado Hernández, M. Alonso Rodrigo, A. J. Àlvarez Barcia, A. Sanchez, V. García Diaz, M. Lopez Peña and J. C. Rodriguez-Cabello, *Regen. Biomater.*, 2019, **6**, 335–347.

57   H. Wang, A. Paul, D. Nguyen, A. Enejder and S. C. Heilshorn, *ACS Appl. Mater. Interfaces*, 2018, **10**, 21808–21815.